surfaces

MDPI

Article

Evaluation of the Surface Finish on 304 Stainless Steel as a Way to Mitigate Calcium Carbonate Scaling

Antônio Carlos Barbosa Zancanella [1,*], Luila Abib Saidler [1], Renato do Nascimento Siqueira [2], Helga Elisabeth Pinheiro Schluter [3] and Bruno Venturini Loureiro [1]

[1] Departamento de Engenharia Mecânica, Universidade Federal do Espírito Santo/Campus Vitória, Av. Fernando Ferrari, 514, Goiabeiras, Vitória 29075-910, ES, Brazil; lusaidler@gmail.com (L.A.S.); bruno.loureiro@ufes.br (B.V.L.)
[2] Instituto Federal do Espírito Santo, São Mateus 29932-540, ES, Brazil; renatons@ifes.edu.br
[3] Petrobras, Rio de Janeiro 20231-030, RJ, Brazil; helga@petrobras.com.br
* Correspondence: antonio.zancanella@ifes.edu.br; Tel.: +55-27-99696-2519 (ext. 29946-580)

Abstract: Calcium carbonate scaling causes significant damage and financial losses to various industries, particularly in deep-water oil exploration. It is affected by factors like pressure, temperature, pH, solution chemistry, and surface finish. Surface finish is critical, as it interacts with the fluid and serves as a substrate for the anchoring of calcium carbonate crystals. However, many studies investigate this phenomenon under conditions that differ from those encountered in deep-water oil exploration. Tests are commonly performed under atmospheric pressure and lacking fluid flow or CO_2 influence, which limits their relevance to industrial conditions. This study aims to evaluate the influence of surface finish on the formation of calcium carbonate scaling under conditions that more closely resemble actual operating environments. 304 stainless steel was selected to replicate industrial conditions, owing to its chemical stability and common use in industrial settings. The tests were conducted in a plant with high-pressure capabilities, operating under continuous flow conditions with CO_2 injection. Controlled surfaces were prepared through metallographic polishing, machining, sandblasting, and laser texturing techniques. Surface characterization was performed using a 3D optical profilometer and scratch testing to measure the average adhesion force. The polymorphs formed were characterized by Raman spectroscopy. Fractal dimension analysis was applied to quantify the complexity of the analyzed surfaces. The results indicate that surfaces with higher fractal dimensions exhibit greater scaling mass and higher adhesion force. The main polymorph observed was calcite. Additionally, it was noted that the texture orientation relative to the flow affects scaling, with higher scaling values observed on surfaces oriented perpendicular to the flow. These findings are crucial for optimizing material selection and surface treatments in deep-water oil exploration, enhancing operational efficiency and reducing costs.

Keywords: scaling; calcium carbonate; surface finish; carbon dioxide injection

check for updates

Academic Editor: Roberto Giovanardi

Received: 19 December 2024
Revised: 25 January 2025
Accepted: 3 February 2025
Published: 7 February 2025

Citation: Zancanella, A.C.B.; Saidler, L.A.; Siqueira, R.d.N.; Schluter, H.E.P.; Loureiro, B.V. Evaluation of the Surface Finish on 304 Stainless Steel as a Way to Mitigate Calcium Carbonate Scaling. *Surfaces* **2025**, *8*, 13. https://doi.org/10.3390/surfaces8010013

Copyright: © 2025 by the authors. Licensee MDPI, Basel, Switzerland. This article is an open access article distributed under the terms and conditions of the Creative Commons Attribution (CC BY) license (https://creativecommons.org/licenses/by/4.0/).

1. Introduction

Scaling is a phenomenon that occurs when inorganic and/or organic material adheres to pipeline walls, partially or completely obstructing fluid flow. Inorganic fouling is common and has significant relevance, as it is present in various segments of industry, from offshore oil extraction, seawater desalination plants, sanitary landfills, and water treatment stations, among other applications, causing a great impact on the productive process [1–3].

Among the problems faced in offshore oil extraction, mineral scaling is one of the phenomena of great relevance, as it reduces the efficiency of the productive process and increases operational costs. The phenomenon of fouling occurs mainly in areas where there is a pressure drop, such as valves, heat exchangers, membranes, measurement instruments, and reductions, obstructing the component and potentially leading to its uselessness. Typically, the phenomenon of scaling can lead to losses on the order of billions of dollars per year for the oil industry [2,3].

In the leachate drainage of sanitary landfills, the low solubility of calcium, combined with the presence of organic material, causes the release of carbon dioxide, favoring the formation of calcium carbonate, thus leading to scaling in drainage pipelines [1].

Some chemical elements have been used as a means to inhibit scaling, achieving good results. However, the observed disadvantages include the occurrence of corrosion in carbon steel equipment, limited action time, and the possible contamination of the water [4–8].

Worldwide, there is a special interest in offshore oil exploration. When analyzing the water present in extraction wells, it was observed that due to the chemical composition, the main scaling is calcium carbonate ($CaCO_3$). Therefore, understanding the factors that govern the formation of calcium carbonate scale holds significant technical and economic importance [9].

Among the variables that influence encrustation, surface finish has a strong influence on calcium carbonate scaling [10–21]. Generally, higher roughness values lead to higher encrustation rates; however, this trend is not always observed. According to studies [10,11], surface roughness alone is an insufficient parameter to relate scaling to surface finish.

Typically, scaling studies use only the average surface roughness R_a or the volumetric roughness S_q [11] for surface characterization [10,13,15,17,19,22–24]. Other authors do not clarify how the roughness analysis was conducted [7,12,14,16,18,25,26]. However, according to [10,11,27], the average roughness R_a is insufficient to characterize a surface, as very distinct surfaces can have the same average roughness value. Thus, the scaling problems addressed require a systematic approach to surface analysis. Various tools for surface characterization are presented and analyzed in the work of [28].

One alternative tool for surface characterization is fractal dimension analysis, which quantifies surface complexity. The higher the fractal dimension, the more intricate the surface, providing a greater area for heterogeneous nucleation [21]. According to [27], fractal dimension provides an accurate description of the complexity of a surface at all roughness scales. In the works of [29,30], methodologies for surface analysis using fractal dimension are presented.

Some of the typical parameters for surface evaluation are R_a, R_{sm}, and R_z. In the discrete case, the R_a value is calculated by summing the absolute values of the heights z_i, measured relative to the mean line at each measurement point, and dividing by the total number of points $\boldsymbol{N}$ [27,28], as shown in Equation (1):

$$R_a = \frac{1}{N}\sum_{i=1}^{N}|z_i| \tag{1}$$

The $\boldsymbol{R_{sm}}$ parameter provides the mean spacing between surface irregularities, calculated as the sum of the adjacent horizontal distances x_i divided by the number of consecutive peaks and valleys $\boldsymbol{M}$ [27,28], as shown in Equation (2):

$$R_{sm} = \frac{1}{M}\sum_{i=1}^{M}|x_i| \tag{2}$$

Another basic parameter for describing a surface is $\boldsymbol{R_z}$. This parameter provides the average height between the five highest peaks $\boldsymbol{p_i}$ and the five deepest valleys v_i relative to a mean line, as shown in Equation (3). It offers an indication of how high the largest peaks and how deep the largest valleys of a surface are [27,28].

$$R_z = \frac{1}{5}\sum_{i=1}^{5}(p_i + v_i) \tag{3}$$

The fractal dimension tool provides a measure of surface complexity and is useful for characterizing rough surfaces, as more complex surfaces have higher fractal dimension (D) values [27,29,30].

The most commonly used method for calculating fractal dimension is the Box-Counting Method, where the surface is divided into a grid of boxes with size $\boldsymbol{\epsilon}$, and the number of boxes $\boldsymbol{N(\epsilon)}$ containing part of the surface is counted; the $\boldsymbol{D}$ is then estimated from the slope of a $\boldsymbol{log(N(\epsilon))\ vs.\ log(1/\epsilon)}$ plot. The fractal dimension tool, also known as texture analysis, is used to quantify the complexity of two-dimensional images, providing a measure that ranges from 1 to 2. For a two-dimensional image to have a well-defined fractal dimension; it must exhibit self-similarity, meaning it displays patterns that repeat across different scales; it must have scalability, where the image retains its properties across varying scales; and it must have complexity, indicating it has a complex structure rather than simply representing a geometric shape [27,29,30].

The choice of method depends on the application and the type of data (2D profile or 3D surface). Modern computational tools, such as surface analysis software, automate these calculations, making the process more efficient and accurate [29,30].

Focusing on the phenomenon of scaling, surfaces with high complexity and elevated roughness values exhibit a larger number of surface cavities, with numerous peaks and valleys, which enhance the propensity for calcium carbonate scale formation [31–36]. Additionally, surface roughness may influence mass transport by inducing a more turbulent regime near the surface, thereby increasing mass transfer and, consequently, promoting greater scaling [23].

The conditions of pressure and temperature are also important, as they can affect the allotropic phase of calcium carbonate, causing the adhesion strength between the substrate and the carbonate to be altered [37].

The studies conducted so far have not been carried out under high-pressure conditions, which are conditions close to those in offshore oil wells [8]. The presence of CO_2 affects the reaction for the formation of calcium carbonate, leading to a greater amount of mineral being formed [38].

Experimental research in the area of encrustation commonly fails to accurately represent the conditions found in oil wells, as turbulence and abrupt variations in thermodynamic parameters are not fully represented under laboratory conditions [25,39,40]. The high pressures found in these environments make it difficult to conduct these studies. Furthermore, most of these experiments are carried out in static tests in reactors or nearly static conditions and by flow in capillary tubes, which often limits the control of flow rates and higher pressure conditions [41]. Another important consideration is understanding the influence of CO_2 on carbonate scaling, as the Brazilian pre-salt presents high levels of CO_2 [42]. The release of CO_2 from the solution is a factor of great importance, from a thermodynamic point of view, in favoring precipitation. CO_2 remains dissolved along with the fluids under pressure and temperature conditions. During a possible depressurization of the system, CO_2 is released from the solution (flash of CO_2), making the medium less acidic and more favorable for the precipitation of $CaCO_3$ [43,44]. It is known that the mass portion of precipitate resulting from the flash of CO_2 can represent up to 85% of

the total amount of precipitated calcium carbonate, compared to the 15% attributed to thermodynamic effects at a temperature of 40 °C [45–48].

The primary objective of this study is to evaluate the influence of surface finish on the formation and adhesion of calcium carbonate scaling under conditions that closely replicate industrial environments, including high-pressure conditions, continuous flow, and CO_2 injection. The study uses 304 stainless steel with varying surface finishes and employs the fractal dimension technique to quantitatively assess the scaling potential of the surfaces.

2. Materials and Methods

2.1. Experimental Setup for the Evaluation of Calcium Carbonate Scaling at High Pressure

The setup used for the tests was built to investigate the scaling phenomenon at high pressures. Figure 1 shows schematic of the system used in the scaling tests.

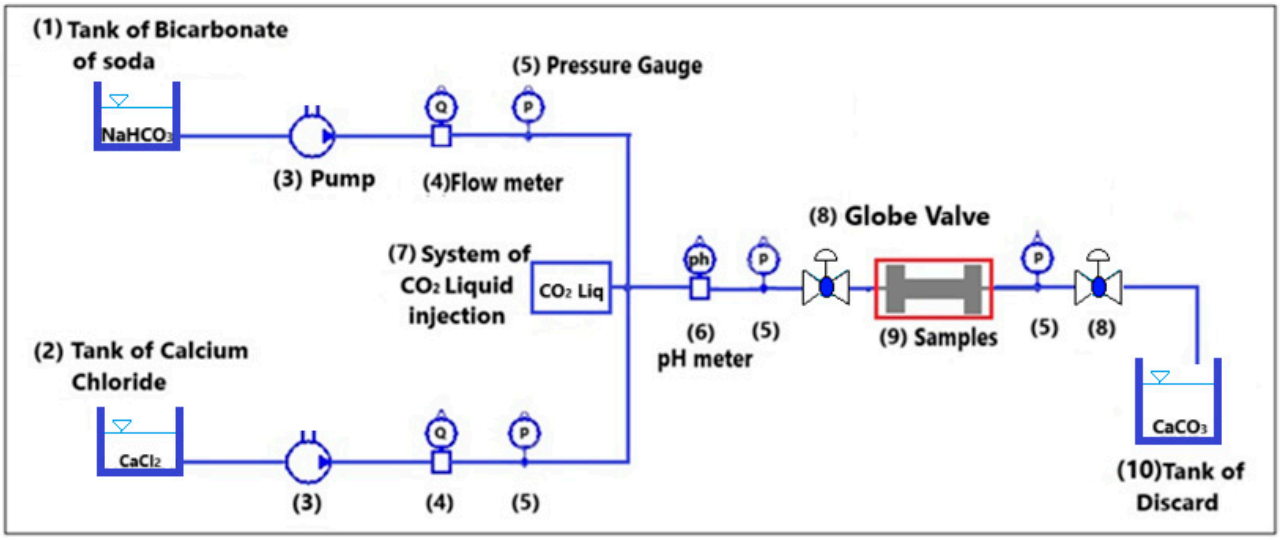


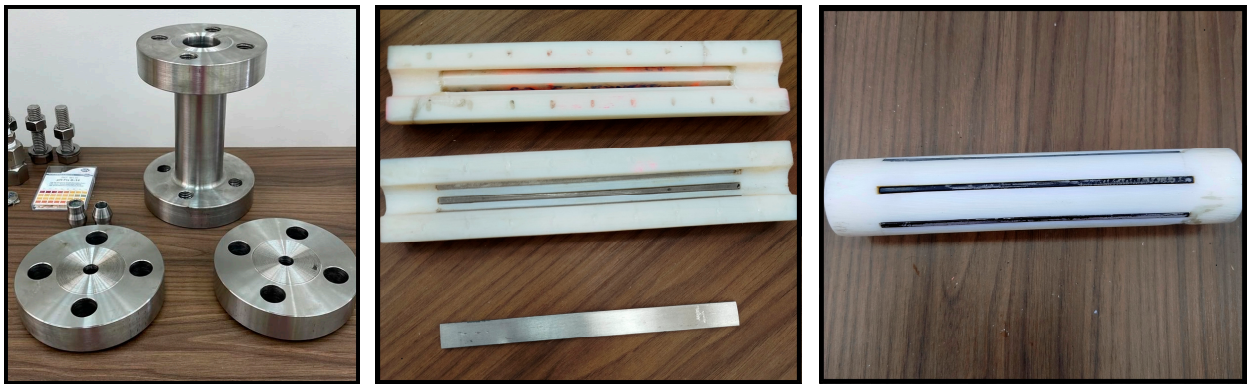
Figure 1. Schematic representation of the experimental scaling plant.

At the beginning of the setup, there are two tanks (1) and (2), where the calcium chloride and sodium bicarbonate solutions are contained. The solutions are pumped individually by high-pressure piston pumps (3) from Bertolini Pumps (Pump, Bertolini, Reggio Emilia, Italy) capable of operating at 500 bar and with a flow rate of up to 600 L/h. The pipes used have a diameter of 3/4 inch and are made of stainless steel 316L. The system includes Coriolis flow meters (Flow Meter, Emerson, MO, USA) (4), with an uncertainty of 0.01 kg/h, a pressure transducer (5) with a capacity of 0–300 bar and an uncertainty of 0.01 bar (Pressure Transducer, Warner, WI, USA), and pH meters (6) with an uncertainty of 0.01 (pH meters, Corr Instruments, Nevada, USA).

The setup includes a liquid CO_2 injection system (7), which mixes with the sodium bicarbonate ($NaHCO_3$) and calcium chloride ($CaCl_2$) lines. After injection, the fluids flow through a section of piping of adequate length to ensure complete solubilization of the CO_2 in the liquid phase. The liquid CO_2 is pressurized by a piston pump.

For pressure control in the analysis section, globe valves are used to control the pressure (8) (Valve, Emerson, MO, USA), with an operating capacity of up to 500 bar and controlled remotely by a pneumatic system. The test specimens are inserted after the control valve (9). Finally, there is the solution disposal tank (10).

The test specimens are connected to the pressure line via a flange system, as illustrated in Figure 2a. In the central region, there is a bipartite cylindrical test specimen cell, as shown in Figure 2b,c, with a capacity for six rectangular prism-shaped test specimens.



(**a**) (**b**) (**c**)

Figure 2. Illustration of the sample coupling system in the line. (**a**) The flanges where the test specimen cell is inserted along with the test specimens. (**b**) The bipartite test specimen cell. (**c**) The assembled cell.

The flange is made of stainless steel 316L, and the assembly of the line is performed with controlled torque using a torque wrench. The cell where the test specimens are inserted is divided into two parts, facilitating handling without damaging the samples after the tests.

The test specimens with different surfaces can be easily manufactured and replaced. The rectangular surface provides a good geometry for subsequent analysis in the 3D optical profilometer.

Figure 3 shows the main parts of the experimental setup. In (Figure 3a), the region where the pumping system and the reservoirs of sodium bicarbonate and calcium chloride solutions are located is shown. In (Figure 3b), the region where the sensors, globe valves, and specimen coupling system are shown.



(**a**) (**b**)

Figure 3. Illustration of the experimental setup. (**a**) The pumping system and solution tanks. (**b**) The location of the sensors, globe valves, and specimen coupling flange.

2.2. Operational Conditions for the Scaling Tests

The experimental control parameters are shown in Table 1, and all samples were tested in triplicate. In the region where the test specimens are inserted, the pressure is reduced to atmospheric pressure in order to optimize the formation of calcium carbonate favoring the phenomenon of CO_2 flash [38,45].

Table 1. Experimental parameters.

Variables	Average	Uncertainty
pH	5.7	0.1
Flow rate of CO_2 injection (kg/h)	3.8	0.9
Flow rate of solutions (L/h)	310.7	2.1
Pressure (bar)	98.8	2.7

2.3. Methodology for the Solution Preparation

The water used for preparing the solutions was treated using a deionizer model CCT-3300 from ROC. The treatment aims to reduce the amount of minerals that are not of interest for analysis, thereby isolating the effect of calcium carbonate.

The solutions were prepared with the objective of optimizing calcium carbonate formation in the line, based on the work [43]. To prepare the 3.67 g/L $CaCl_2$ solution, the mixing tank was filled with 1000 L of deionized water (volume verified by the totalizer), 3.67 kg of $CaCl_2 \cdot 2H_2O$ was weighed using a Marte LS20 balance and added to the mixer. The mixture was allowed to homogenize for 1 h and then transferred to the IBC tank. After 7 days, the solution was ready for use.

To prepare the $NaHCO_3$ solution with a concentration of 6.30 g/L, the mixing tank was filled with 1000 L of deionized water (volume verified by the totalizer), 6.30 kg of $NaHCO_3$ was weighed on a Marte LS20 balance and added to the mixer. The mixture was allowed to homogenize for 1 h and then transferred to the main tank. The solution was rested for 7 days for the solvation of the reagents. The methodology for preparing the solution was based on the work of [43].

2.4. Fabrication of the Test Specimens

The test specimens were fabricated from stainless steel 304, with dimensions of 150 mm in length, 12.9 mm in width, and 3.3 mm in thickness. 304 steel was chosen for its chemical stability and extensive industrial applications. The specimens were obtained from a flat bar measuring 12.9 mm in width, 3.3 mm in thickness, and 6 m in length. The samples were cut using a metallographic cutter.

To produce different surface finishes, four techniques were used: metallographic polishing, machining, sand blasting, and laser texturing, resulting in eleven distinct types of surfaces: two polished, six machined, one blasted, and two laser-textured surfaces.

Two polished surfaces were produced using the metallographic polishing process, one with a mirror finish, where polishing was performed with alumina with a particle size of 4 μm, and the other with a rougher surface, where polishing was completed with 400-grit sandpaper. For the metallographic polishing, a Struers DP3 machine was used (Polisher, Struers, Ballerup, Denmark) maintaining a rotation of 300 RPM, and the sandpapers used were 400, 800, and 1200 grit, and finally alumina with a particle size of 4 μm.

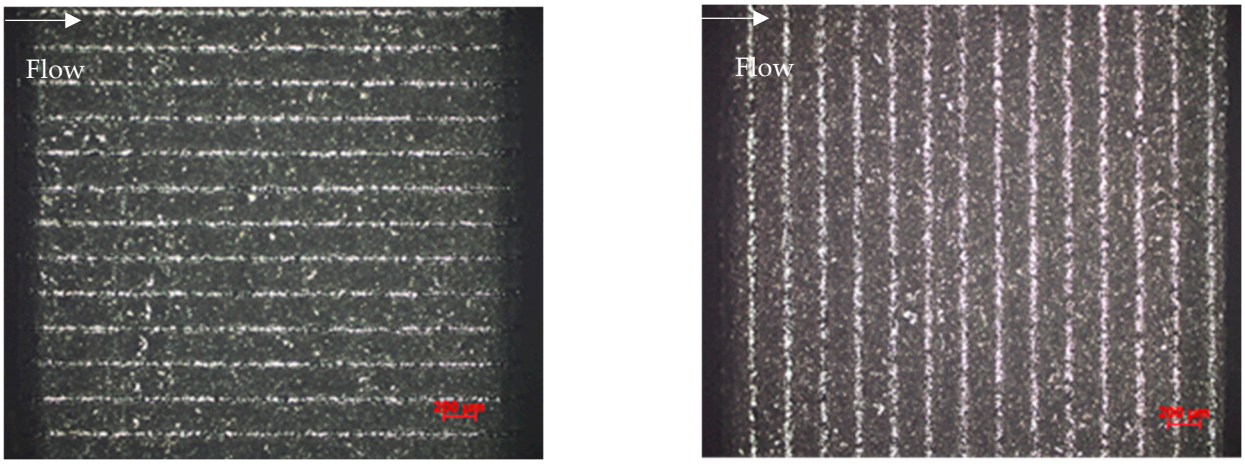
To vary the surface finish on the machined surfaces, a DPT FU301 milling machine was used (Milling Machine, Promil, São Paulo, Brazil). In all cases, a rotation of 1000 RPM and a cutting depth of 0.2 mm were employed. The parameters used for milling are displayed in Table 2, where M1–M6 are the machined samples. The tool used was a 17 mm diameter titanium-coated end mill with four cutting edges.

To fabricate the test specimens with laser texturing, the equipment used was the Scanlab brand, model BasiCube 10 (Laser texturing, Scanlab, Puchheim, Germany) which operates at a wavelength of 1064 nm. The spacings produced via laser were made uniformly, measuring 200 μm, in both the longitudinal and normal directions to the flow. Figure 4 illustrates the surface finish of the samples produced via laser. The images were obtained

using an Eclipse MA200 optical microscope (Microscope, Nikon, Tokyo, Japan). The textures are observed in two directions, longitudinal and normal relative to the flow, both with an average spacing of 200 µm.

Table 2. Machining parameters used.

Machined Test Specimens	M1	M2	M3	M4	M5	M6
Cutting Speed (mm/min)	63	125	250	315	500	630



(**a**) (**b**)

Figure 4. Samples with laser-structured surfaces, viewed under a microscope at 100× magnification; (**a**) textures oriented longitudinally and (**b**) textures oriented transversely.

2.5. Surface Characterization and Detachment Force

For surface characterization, the 3D optical profilometer Sensofar, model NEOX SS-NEOXOO was used. The analysis was conducted according to the ISO 21920 standard [49], and the region of the analyzed surface was 5500 µm by 650 µm. For each type of test specimen, five distinct samples were analyzed, where the average values of their properties were evaluated.

It is also important to highlight the significance of the surface area used in predicting roughness values, as roughness varies depending on the size of the analyzed region. Since roughness values depend on the analyzed area, it is crucial to specify the area used when comparing results with other studies.

In the analysis of the scaling mass with different surface finishes, the parameters of fractal dimension (dimensionless) R_a, R_z, and R_{sm} were selected. The parameters used were obtained according to [28,29]. The measurements and procedures performed are based on the ISO 21920 standard [49].

For the calculation of the fractal dimension, surface images were analyzed using ImageJ software (version 1.53t) with the Fractal Box Count tool. The surfaces exhibited characteristics of self-similarity, scalability, and complexity, allowing for the assignment of fractal dimension values. Five regions from each sample were analyzed, with standardized resolution across all surfaces, and the mean and standard deviations of the quantities of interest were extracted.

To ensure consistent surface comparison, all images must have the same resolution. In this case, they were obtained via profilometry at a resolution of 1377 pixels by 1136 pixels. Figure 5 displays the image of machined surface 1. The image was converted to 8-bit, and the contrast was adjusted to enhance the visualization of surface details. Subsequently, the Box-Count tool was applied to calculate the fractal dimension value. The

fractal dimension of the surfaces represents the degree of surface complexity, which is proportional to the number of voids and surface reliefs that may serve as anchoring sites for calcium carbonate crystals.

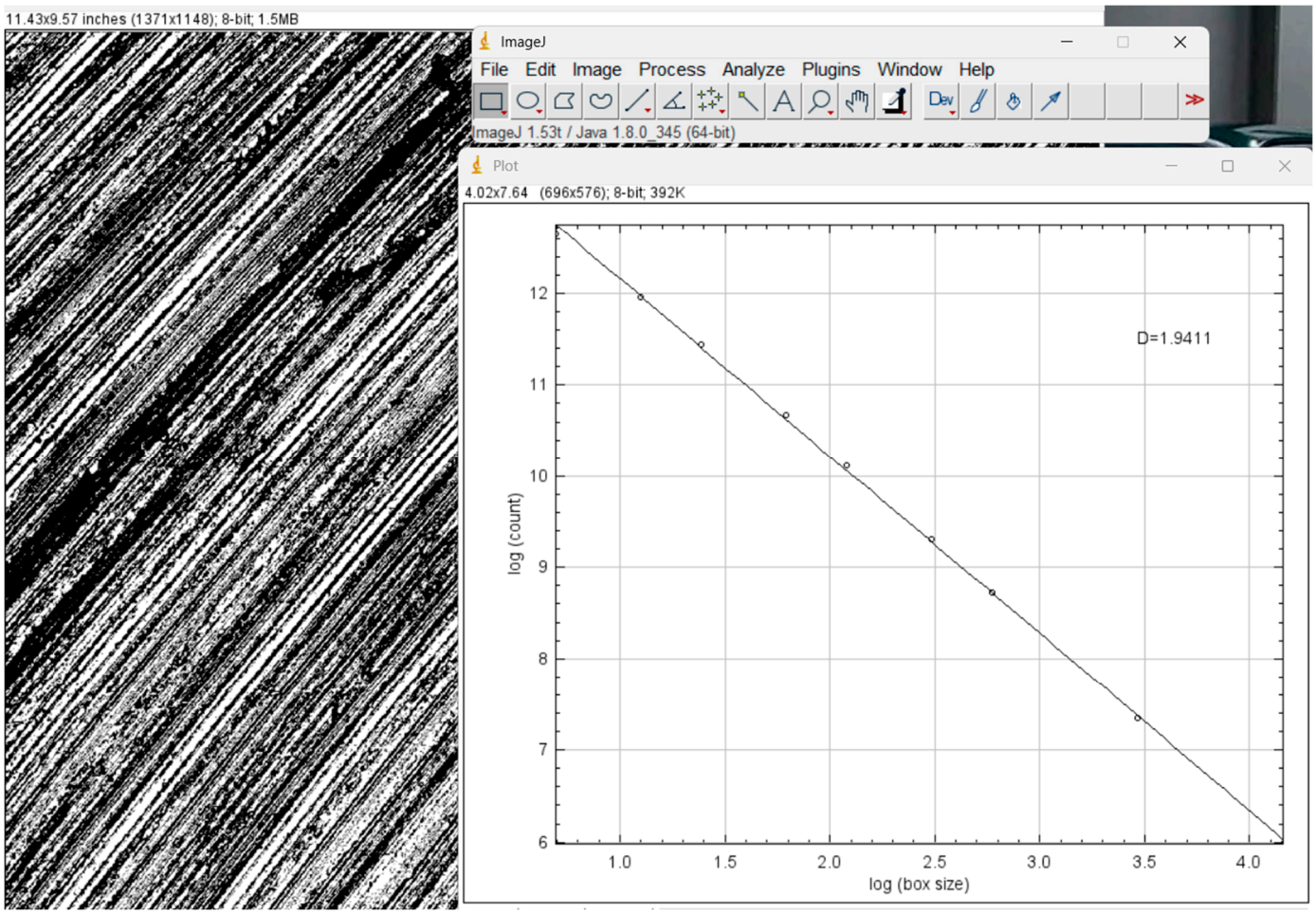


Figure 5. An example of image processing and fractal dimension analysis.

To estimate the mechanical resistance of the calcium carbonate film, the technique of sclerometry was used. The equipment utilized was an APEX (Sclerometry, CETR/Bruker, MA, USA). All tests were conducted with a length of 20 mm, a speed of 0.167 m/s, a Rockwell C-type indenter, a load application rate of 1 N/mm, and a pre-load of 0.5 N. The standards used as references were ASTM C1624-22 [50] and ASTM G171-03 [51].

The detachment force was estimated by measuring the distance of the scratch produced, multiplied by the loading rate (1 N/mm), plus the value of the pre-load (0.5 N). For this purpose, a Zeiss Stereo Discovery V20 microscope was used (Microscope, Zeiss, Oberkochen, Germany). For each type of surface, five scratches were made, and the average force values for each surface type were obtained. The tests were conducted in triplicate.

2.6. Analysis of Encrusted Mass and Polymorphism

The analysis of the mass of calcium carbonate encrusted was performed using the gravimetric method. After the tests, the specimens were removed from the mold (Figure 4). The unwanted encrustation, not located on the surface of interest, was removed using 10% acetic acid with the aid of a cotton swab on all samples. Subsequently, the samples were dried at room temperature for 24 h in a glass desiccator. The mass measurement was conducted using an analytical balance model MS304TS/A00 (Analytical Balance, Toledo, OH, USA), with an uncertainty of 1 mg.

For the characterization of the polymorphs of calcium carbonate, the Raman spectroscopy technique was used with an Alpha300 A model (Atomic Force Microscope, WITec GmbH, Ulm, Germany).

3. Results and Discussion

The analysis of the surface at a microscopic level allows an understanding of how the interaction with the fluid occurs and how its interstices can accommodate particulate material and facilitate the nucleation and growth of crystals. This contributes to a better understanding of how the phenomenon of scaling develops, enabling the mitigation of its effects through the control of surface characteristics.

The proposed surfaces were analyzed using profilometry, exhibiting quite distinct morphological characteristics (Figure 6 and Table 3). The polished surface (Figure 6a) presents a flat aspect and a low roughness value compared to the others. This surface exhibits an isotropic characteristic with low-frequency roughness and peaks and valleys with a maximum height R_z on the order of 1 µm. In contrast, the sanded surface (Figure 6b) displays high-frequency roughness with peaks and valleys having a maximum height R_z on the order of 10 µm, and it also has isotropic characteristics.

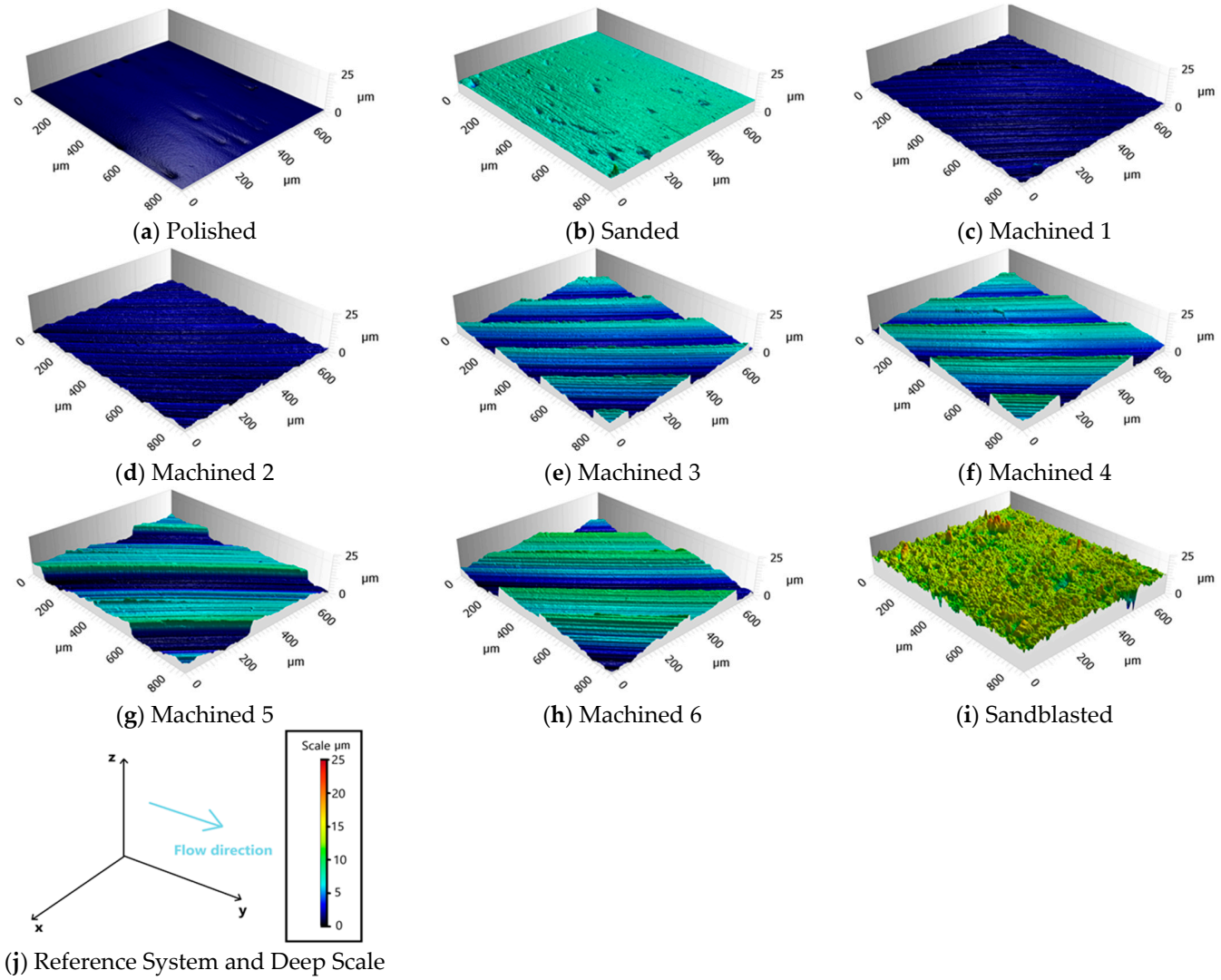


Figure 6. Analyzed surfaces (**a**–**i**) and reference and scale system (**j**).

Table 3. Surface parameters of the test specimens used.

Test Specimens	Fractal Dimension	R_a (µm)	R_{sm} (µm)
Polished	1.1015	0.03	140.1
Sanded surface	1.3221	0.18	70.6
Machined 1	1.9523	0.31	50.4
Machined 2	1.8507	0.42	55.4
Machined 3	1.8389	1.21	122.2
Machined 4	1.7943	1.40	143.7
Machined 5	1.9166	1.73	167.8
Machined 6	1.8455	2.06	203.2
Sand Blasted	1.9733	1.02	51.8

The complexity of the two surfaces produced by metallographic polishing (Figure 6a,b) was low compared to the subsequent samples. The polished surface exhibited a fractal dimension of 1.1015 (dimensionless), while the sanded surface had a value of 1.3221. Both surfaces appeared flat compared to the others, resulting in reduced interaction with the flowing fluid.

The machined surfaces (Figure 6c–h) exhibit a periodic surface pattern, characteristic of the manufacturing process. It was observed that as the cutting speed increased, the peaks and valleys become wider and deeper. The machined surface with the lowest feed rate (Machined 1, Figure 6c) had an average roughness $\boldsymbol{R_a}$ of 0.31 µm and a $\boldsymbol{R_z}$ of 1.85 µm. In comparison, the machined surface with the highest feed rate (Machined 6, Figure 6h) had a $\boldsymbol{R_a}$ roughness value of 2.06 µm, and the average height of the peaks and valleys $\boldsymbol{R_z}$ is 5.06 µm. It is noted that although the average roughness and average height increase with the feed rate, the surface with lower roughness exhibits a higher number of peaks and valleys within the same analyzed area. The average alignment of the machined surfaces concerning the flow was 45°.

Still regarding the machined surfaces, when analyzing surface complexity, samples with lower roughness values (lower feed rates) exhibited lower fractal dimension values, indicating that these surfaces are more complex, with a large number of peaks and valleys, which can facilitate the scaling of calcium carbonate. The highest fractal dimension value was 1.9523, obtained from machined surface 1, while the lowest value was displayed on machined surface 4 (Figure 6f), with a value of 1.7943; as observed, the fractal dimension value does not follow a linear trend with the cutting speed used in surface fabrication (See Table 3).

Lastly, regarding the sandblasted surface (Figure 6i), an irregular and isotropic pattern is observed, which is characteristic of the abrasive blasting process. This surface exhibited an average roughness $\boldsymbol{R_a}$ of 1.02 µm, with a maximum height $\boldsymbol{R_z}$ on the order of 10 µm. In terms of complexity compared to the others, this surface had the highest value, displaying a fractal dimension of 1.9733. The number of interstices on this surface may be a predominant factor in achieving high levels of embedded mass on this type of surface; they can also provide a large anchoring area, thereby making the removal of encrustation more difficult, which translates into high values of force required for the removal of inorganic materials, as will be discussed later.

The laser-produced surfaces were analyzed separately due to the nature of the manufacturing process used to create their textures.

The obtained values of fractal dimension, $\boldsymbol{R_a}$ roughness, and peak and valley widths $\boldsymbol{R_{sm}}$ for each surface are summarized in Table 3. It can be observed that the polished surface exhibits the lowest $\boldsymbol{R_a}$ roughness and the lowest fractal dimension value, followed by the sanded surface. The machined surfaces from 1 to 6 show increasing $\boldsymbol{R_a}$ roughness; however, the fractal dimension did not follow this order, achieving higher values in test specimens 1

and 5. The pattern left on the machined surface results from the interaction with the cutting tool and does not necessarily exhibit a fractal dimension proportional to the feed rate. Explanations include heat transfer, tool-material interaction, altered metal deformation mechanisms, and interaction with the removed material. A more detailed discussion is beyond the scope of this work, and further data are required for comprehensive analysis. Finally, the highest fractal dimension value was obtained for the sandblasted surface. The table also includes the average values of peak and valley widths (R_{sm}). Among the machined surfaces, there is an observed increase in the average width of peaks and valleys with the increase in cutting tool feed rate, obtaining the highest value in the machined surface 6.

Surface energy is also commonly used to evaluate the effect of the surface on calcium carbonate scaling [13,15]. However, the analyzed surfaces have the same chemical composition as the substrate, making the variation imperceptible. In the work of [15], different materials with varying chemical compositions are evaluated, but this study emphasized the effect of roughness only, maintaining the same material, which was stainless steel 304.

One notable aspect of the roughness measurements is the range of finishes used. In [13], the range was 0.2–1.91 µm, while in the present work, the range utilized was 0.03–2.06 µm. Additionally, the study in [12] employed a smaller range of roughness values, specifically 0.01–0.1 µm. In this work, a broad range of roughness values was targeted for scaling tests, ensuring compatibility with those commonly found in typical manufacturing processes.

In addition to roughness, the orientation of the surface in relation to the main flow (Figure 6j) should also be discussed, which was not explicitly addressed in the analyzed studies (except for [11], which evaluated the effect of roughness orientation relative to the flow). The orientation of the surface roughness in relation to the flow affects how the fluid interacts with the surface, potentially modifying mass transport characteristics, either promoting or hindering the scaling phenomenon.

The scaling experiments were conducted with controlled parameters as specified in Table 2. Triplicate tests were performed for all specimens tested.

After completing the surface characterization, bench tests were conducted using a pressurized system to evaluate the influence of the surface on the scaling process. Figure 7 shows the scaling mass (m) for each analyzed roughness R_a. It can be observed that there is no clear pattern regarding how the surface affects the deposited mass. Among the machined specimens tested, the surface with the lowest roughness exhibited a higher scaling mass, while the surface with the highest roughness showed a lower scaling mass. In the polished samples, despite the significant difference in finishing, the scaling mass values were statistically similar.

The surface that exhibited the highest mass of scale deposition was the shot-blasted one, even though it did not have the highest average roughness R_a. These results indicate that the roughness parameter R_a is insufficient for evaluating the scaling effect. As an average value, R_a provides limited information about the analyzed surface, as different surfaces with distinct characteristics can exhibit the same R_a value according to [27].

In contrast to the present study, the research conducted by [11] concluded that roughness did not significantly affect the scaling mass of calcium carbonate. However, the tests were carried out with a narrower range of roughness compared to the one used in this work.

Unlike the present study, where no clear pattern of variation in the scaling mass as a function of the average roughness R_a was observed, the works of [12,13,15,19,22,40] associate the increase in deposited mass with the increase in average roughness. It is worth noting that these studies used a smaller range of roughness and different surfaces. The tests were also conducted under different conditions, such as low pressure and the absence

of CO_2 injection, which makes them less representative of the actual scaling conditions in the industry.

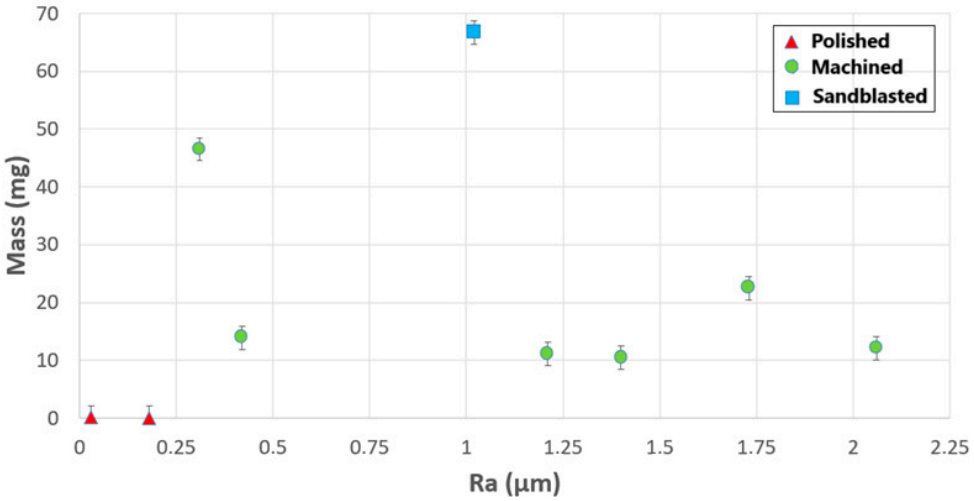


Figure 7. Variation of the deposited mass with the average roughness R_a for the different analyzed surfaces.

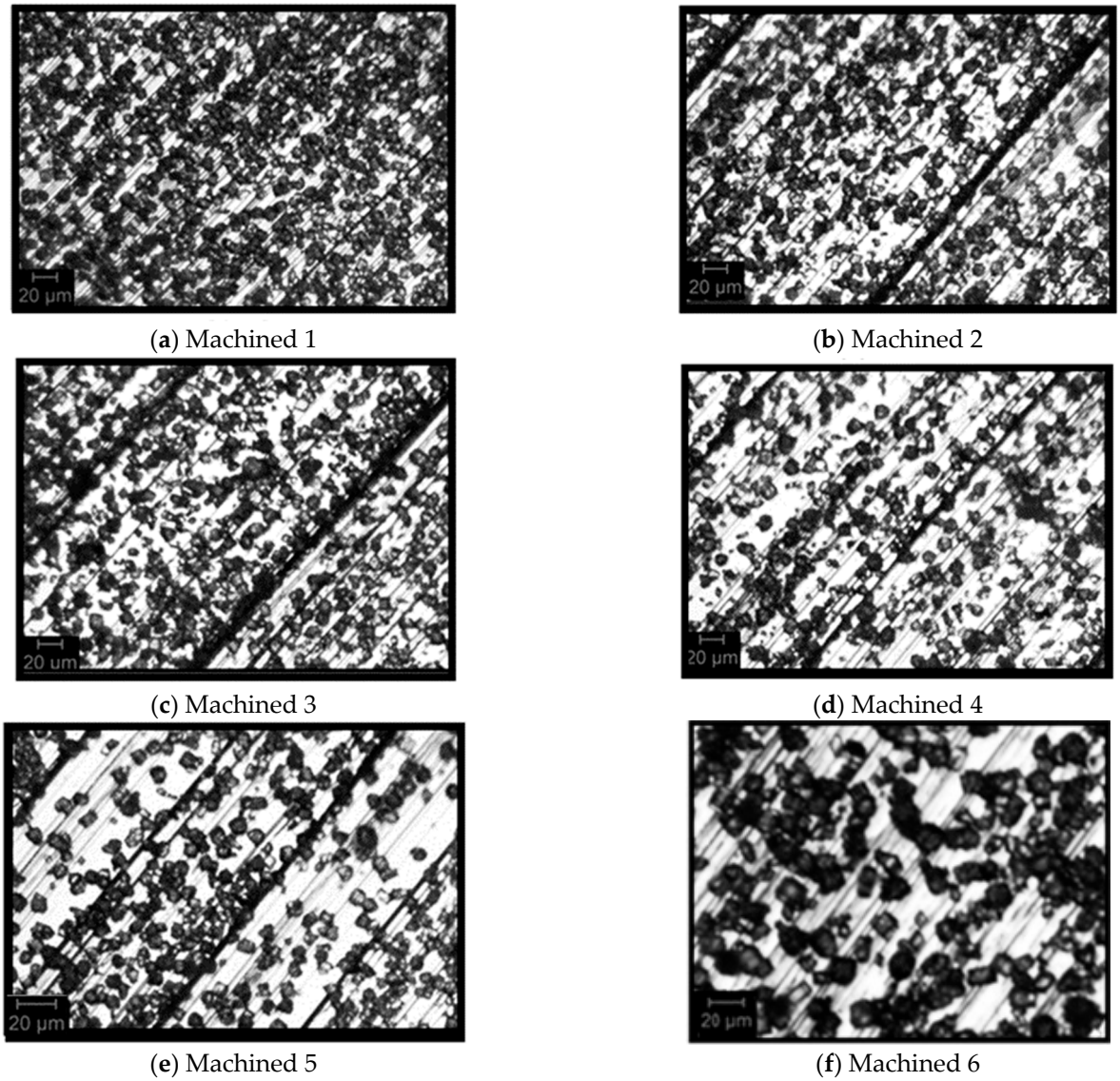
Unlike the study presented herein, several authors have employed multiple materials as substrates [12,15,19], which complicates the isolation of the roughness effect, given that the chemical properties of the materials also significantly influence the scaling process. In the current study, 304 stainless steel was selected to mitigate the impact of corrosion, a phenomenon that may interfere with the scaling process and introduce an additional variable, potentially leading to misleading results. For example, in the study by [22], tests were conducted using ***ASTM 1020*** carbon steel, a material prone to corrosion when exposed to salts such as calcium carbonate, which could compromise the interpretation of scaling behavior.

Regarding Figure 7, within the same surface class (green circular points), no linear pattern of scaling was observed with the roughness R_a; the complexity of the surfaces cannot be represented by an average parameter. It is noted that the machined surface 1 had greater scaling than the others. When observed under the microscope (Figure 8a), it was found that the dimensions of the peaks and valleys of this surface better anchored the calcium carbonate crystals compared to the other surfaces.

Similarly to R_a, it was found that R_z and R_{sm} also do not provide an accurate description of a surface's scaling potential.

It should be noted that the rougher surfaces, which were produced with higher feed rates, have wider peaks and valleys that do not accommodate the calcium carbonate crystals as effectively, making them more easily removed by the flow (Table 3 and Figure 6). The parameter used to quantify the average width of the peaks and valleys of a surface was R_{sm}, which varies from 50.4 µm on the machined surface 1 to 203.2 µm on the machined surface 6. It can be observed that the crystals have a width compatible with the peaks and valleys of machined surface 1.

It can also be observed that from machined surface 1 to machined surface 6, there was a decrease in the quantity of crystals (Figure 8); although, their size increased, which is a result that aligns with the observations made by [11]. As the width of the peaks and valleys increased, especially on surfaces 5 and 6, there was a decrease in the number of crystals accommodated on the surface, as they were carried away by the flow.



(**a**) Machined 1 (**b**) Machined 2

(**c**) Machined 3 (**d**) Machined 4

(**e**) Machined 5 (**f**) Machined 6

Figure 8. Machined surfaces after the 30-min encrustation test.

Upon observing Figures 7 and 8, it is noted that the scaling mass did not follow a linear trend with roughness. Despite the different testing conditions, this result is consistent with the experiments conducted by the authors in [21].

As discussed thus far, the average roughness was unable to correlate the phenomenon of encrustation with surface finish. Therefore, the use of the mathematical tool of fractal dimension is proposed to quantify the complexity of the surfaces. Figure 9 displays the mass (m) of calcium carbonate encrusted against the fractal dimension (D) of the evaluated surfaces. An increase in the mass of encrustation is observed with the increase in surface complexity; more complex surfaces show a greater scaling tendency.

Higher fractal dimension values are associated with larger surface areas, consequently providing a greater area for anchoring and growth of calcium carbonate crystals, a fact that agrees with the observations made by [13].

Surfaces with higher fractal dimension values exhibit greater irregularity, which may intensify their interaction with the flowing fluid. This interaction could modify the formation of the boundary layer near the surface, resulting in a more turbulent and diffusive flow. Consequently, the mass of calcium carbonate adhered to the surface increases. These explanations align with the results reported in [21,23].

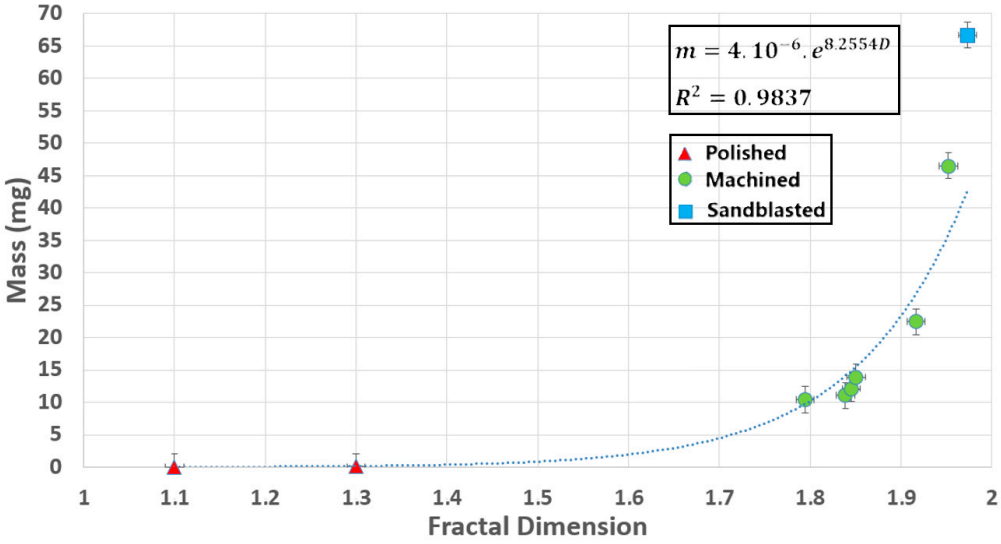
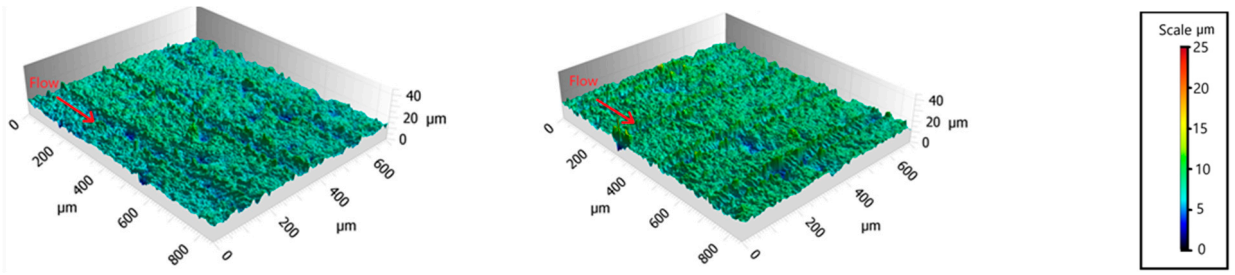


Figure 9. Variation of the encrusted mass with the fractal dimension.

Another factor that deserves attention is the influence of the surface orientation relative to the flow. For this purpose, two surfaces were produced by the laser texturing process. The surfaces are considered statistically identical, with the same R_a value of 1.2 ± 0.4 µm and the same fractal dimension of 1.9601 ± 0.010 µm. Figure 10 shows the laser-produced surfaces, with orientation parallel to the flow (Figure 10a) and normal to the flow (Figure 10b), as well a deep scale color (Figure 10c).



(**a**) Textures parallel to the flow (**b**) Textures normal to the flow (**c**) Deep Scale

Figure 10. Profilometry of the samples produced via laser, with (**a**) horizontal orientation to the flow (parallel to the flow), (**b**) normal orientation (perpendicular to the flow), (**c**) Deep scale color).

The mass results obtained were higher in the test specimens oriented perpendicular to the flow, with a scaling mass of 61.7 ± 0.1 mg, compared to 16.7 ± 1 mg for surfaces with parallel textures. These results highlight that, depending on the orientation of the surface roughness, different scaling mass results can be observed, even for statistically identical surfaces. Therefore, it is important to also consider the flow direction in relation to the texture of the roughness imposed on the surface.

The surface that is oriented parallel to the flow of the solution will tend to disturb the flow less, making it less turbulent and consequently less diffusive, leading to lower encrustation values. These results may vary as the velocity values are altered, in accordance with what has been discussed by [21,23].

In contrast, [11] concluded that the texture parallel to the flow exhibited a higher scaling mass. However, it should be noted that the flow conditions in the studies are entirely different, as the authors used a magnetic stirrer to generate the flow, which may lead to significant differences compared to the flow presented in the present study. Furthermore, it should be noted that the test conditions were completely distinct, as they were conducted by the authors at atmospheric pressure and without CO_2 injection.

To conclude the discussion about surface orientation, it is important to highlight that the phenomenon of scaling is complex and should be analyzed with the aid of various surface parameters. As observed, even with the same fractal dimension, changing the orientation of the textures resulted in different values of encrusted mass. For scaling mass analysis, fractal dimension proved to be a useful tool, providing a consistent relationship between the increase in scaling mass and surface complexity, being more efficient than the traditional R_a parameter. However, for surface description, without relation to scaling mass, it is still necessary to use traditional surface parameters like R_a, R_z, and R_{sm}. Nevertheless, these parameters alone are not good estimators of scaling potential.

An important measure that complements the study of scaling is the detachment force. Figure 11 shows the results of the detachment force measured for the selected samples. It can be observed that the detachment force on the sandblasted surface was the highest among all samples. Among the machined surfaces, machined surface 1 exhibited the highest detachment force. The graph also presents the fractal dimension values for the samples. It is noted that higher fractal dimension values lead to greater detachment force values, as they are associated with larger amounts of interstices for anchoring calcium carbonate crystals, necessitating a greater force to detach them.

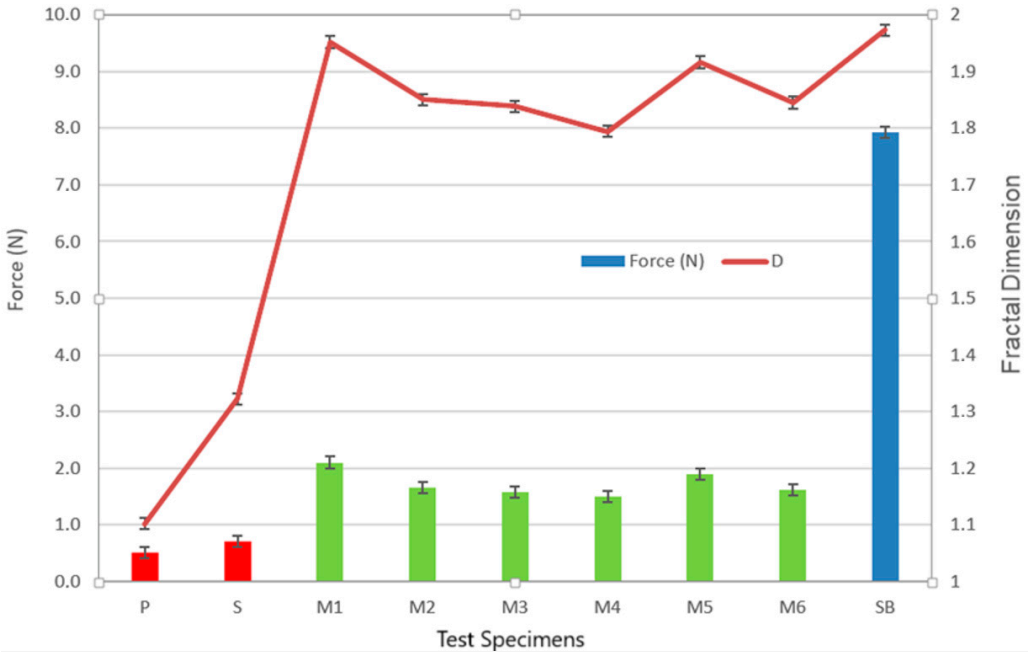


Figure 11. Detachment force (N) and fractal dimension for the evaluated test specimens, where P is the polished specimen, S is the sanded specimen, M1–M6 are the machined specimens, and SB is the blasted specimen.

Another important observation is that, in machined samples 1 and 5 and the blasted one, the fractal dimensions, although seemingly similar, lead to varying detachment force results. It is worth noting that the fractal dimension is a parameter ranging from 1 to 2 in two-dimensional images, and even small variations in this parameter can lead to significant changes in surface properties (Table 3). Machined surfaces exhibit a periodic and well-defined texture, with patterns determined by the manufacturing process (Figure 6). In contrast, the blasted surface displays an isotropic character, with more interstices and smaller dimensions, which promotes stronger adhesion of the calcium carbonate film compared to the machined surfaces.

These results are consistent with findings from [13,15,20], where surfaces with a high degree of complexity exhibited greater adhesion forces. It is noted that surfaces with high levels of scaling also demonstrate elevated values of detachment force.

In the study by [20], it is discussed that the interaction force between calcium carbonate and the surface is of the van der Waals type, where substrates with greater interaction forces exhibit higher adhesion forces. Additionally, greater interaction was observed on complex surfaces with higher surface area values, which also corresponded to higher fractal dimensions.

Another important variable in the study of calcium carbonate scaling is the polymorph present, as this variable influences surface adhesion. Regarding the polymorphism of the obtained calcium carbonate, it was observed through Raman spectroscopy (Figure 12) that the polymorph obtained was calcite. This result is consistent with the findings of [46–48].

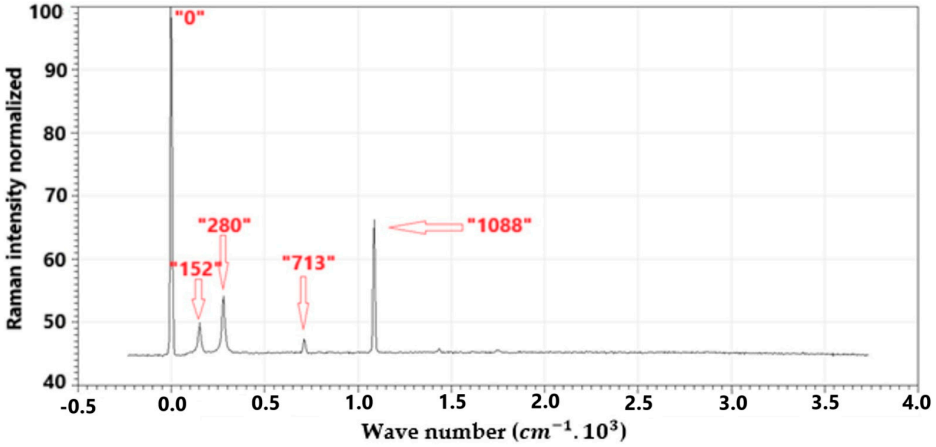


Figure 12. Raman spectroscopy curve of the calcium carbonate obtained in the tests.

The result of the Raman spectroscopy is confirmed by the microscopy images of the calcium carbonate obtained in the experiments, where calcite is observed as the main polymorph in rhombohedral form (Figure 13). Although the experiments were conducted dynamically, with continuous pressurized flow, the results agree with theoretical predictions and static tests performed by other authors [31,32,34,36,37]. For the pressure and temperature in which the experiments were conducted, calcite is expected to be the thermodynamically stable polymorph.

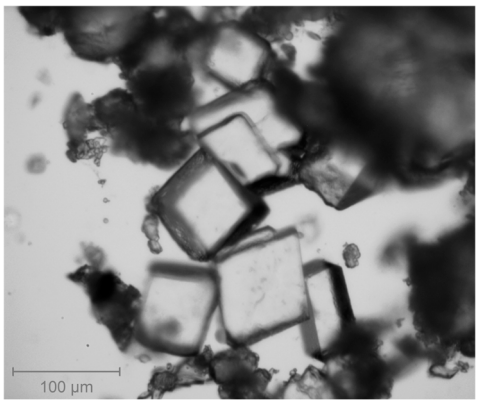


Figure 13. Calcite polymorph resulting from the experiments, which has a rhombohedral structure.

4. Conclusions

The use of surface roughness R_a as a way to quantify the potential for scaling on a surface is insufficient, as it does not describe the details of a surface. Within the range

of roughness evaluated, its utilization did not provide a well-defined trend, making it a poor estimator of encrustation potential, providing a misleading notion of following a trend in certain ranges. In the experiments, a good correlation was observed between the scaling mass and the fractal dimension, making it a good estimator of a surface's scaling potential. Even so, for surface description and analysis, it is still necessary to use basic parameters such as R_a, R_z and R_{sm}. The complexity of a surface is related to the number of available sites and area for the occurrence of encrustation. It was observed that surfaces with higher scaling mass values, resulting from a high fractal dimension, also exhibited elevated values of detachment force of the calcium carbonate film. It was noted that statistically identical surfaces, oriented differently in relation to the flow, did not exhibit the same encrustation mass, highlighting the importance of not only fractal dimension and roughness measurements for surface characterization but also the orientation of surface textures concerning the flow.

Author Contributions: Conceptualization, A.C.B.Z., R.d.N.S., H.E.P.S. and B.V.L.; methodology, A.C.B.Z., L.A.S. and R.d.N.S.; software, A.C.B.Z. and R.d.N.S.; validation, A.C.B.Z.; formal analysis, A.C.B.Z., L.A.S. and R.d.N.S.; investigation, A.C.B.Z. and R.d.N.S.; resources, H.E.P.S.; writing—original draft, A.C.B.Z.; writing—review and editing, R.d.N.S.; supervision, R.d.N.S., H.E.P.S. and B.V.L.; project administration, L.A.S., H.E.P.S. and B.V.L. All authors have read and agreed to the published version of the manuscript.

Funding: The research received external support from the company Petrobras.

Data Availability Statement: Data is contained within the article.

Conflicts of Interest: Author Helga Elisabeth Pinheiro Schluter were employed by the company Petrobras, Rio de Janeiro 20231-030, RJ, Brazil. The authors declare that the research was conducted in the absence of any commercial or financial relationships that could be construed as a potential conflict of interest.

References

1. Zhao, R.; Chen, J.; Liu, J.; Li, M.; Yang, H. Anti-Scaling Performances of Different Aged Landfill Leachates on PPR and ABS Pipe Materials. *Water Sci. Technol.* **2023**, *87*, 366–380. [CrossRef]
2. Lai, N.; Wen, Y.; Wang, Y.; Zhao, X.; Chen, J.; Wang, D.; Jia, C. Calcium Carbonate Scaling Kinetics in Oil-field Gathering Pipelines by Using a 1D Axial Dispersion Model. *J. Pet. Sci. Eng.* **2020**, *188*, 106925–106937. [CrossRef]
3. Zanacic, E.; McMartin, D.W. Calibration and Validation of Calcium Carbonate Precipitation Potential (CCPP) Model for Strontium Quantification in Cold Climate Aquatic Environments. *Environments* **2022**, *9*, 74–83. [CrossRef]
4. Alhalili, Z.; Souli, H.; Smiri, M. Effect of LEO (Lycium Essential Oils) as Green Inhibitors of Calcium Carbonate Scale on Nanoparticles-Doped Ultrafiltration Membrane (UFM) and Water Treatment. *Arab. J. Sci. Eng.* **2022**, *47*, 6233–6243. [CrossRef]
5. Kamal, M.S.; Hussein, I.; Mahmoud, M.; Sultan, A.S.; Saad, M.A. Oilfield Scale Formation and Chemical Removal: A Review. *J. Pet. Sci. Eng.* **2018**, *171*, 127–139. [CrossRef]
6. Kohler, N.; Courbin, G.; Ropital, F. Static and Dynamic Evaluation of Calcium Carbonate Scale Formation and Inhibition. In Proceedings of the SPE European Formation Damage Conference, OnePetro, The Hague, The Netherlands, 21 May 2001.
7. Teng, K.H.; Kazi, S.N.; Amiri, A.; Habali, A.F.; Bakar, M.A.; Chew, B.T.; Khan, G. Calcium Carbonate Fouling on Double-Pipe Heat Exchanger with Different Heat Exchanging Surfaces. *Powder Technol.* **2017**, *315*, 216–226. [CrossRef]
8. Hamid, S.; De Jesús, O.; Jacinto, C.; Izetti, R.; Pinto, H.; Droguett, E.; Batocchio, M. A Practical Method of Predicting Calcium Carbonate Scale Formation in Well Completions. *SPE Prod. Oper.* **2016**, *31*, 1–11. [CrossRef]
9. Cosmo, R.P. Modelagem e Simulação Termodinâmica da Precipitação de Calcita em Condições de Poço. Master's Thesis, Programa de Pós-Graduação em Energia, Universidade Federal do Espírito Santo, São Mateus, Espírito Santo, Brazil, 2013.
10. Cheong, W.C.; Neville, A.; Gaskell, P.; Abbott, S. Using Nature to Provide Solutions to Calcareous Scale Deposition. In Proceedings of the SPE International Oilfield Scale Conference, OnePetro, Aberdeen, Scotland, 28 May 2008.
11. Jin, H.Q.; Athreya, H.; Wang, S.; Nawaz, K. Experimental Study of Crystallization Fouling by Calcium Carbonate: Effects of Surface Structure and Material. *Desalination* **2022**, *532*, 115754–115761. [CrossRef]
12. Sun, N.; Jiang, H.; Liang, A.; Zhang, D.; Cai, H.; Zhang, L.; Chong, X. Influences of Material Types on the Mechanisms of Crystal Growth in an Aggregate Scaling Device. *Int. Commun. Heat Mass Transf.* **2019**, *108*, 104303–104312. [CrossRef]

13. Al-Gailani, A.; Charpentier, T.V.; Sanni, O.; Neville, A. Crystallization Fouling in Domestic Appliances and Systems. *Heat Transf. Eng.* **2021**, *43*, 1301–1310. [CrossRef]
14. Charpentier, T.V.; Neville, A.; Baudin, S.; Smith, M.J.; Euvrard, M.; Bell, A.; Barker, R. Liquid Infused Porous Surfaces for Mineral Fouling Mitigation. *J. Colloid Interface Sci.* **2015**, *444*, 81–86. [CrossRef] [PubMed]
15. Cheong, W.C.; Gaskell, P.H.; Neville, A. Substrate Effect and Surface Adhesion/Crystallization of Calcium Carbonate. *J. Cryst. Growth* **2013**, *363*, 7–21. [CrossRef]
16. Dilsiz, E.A.; Mihcakan, I.M. The Effects of Calcium Carbonate Precipitation on High-Velocity Flow Behavior in 3D Printed Fracture Models. *Geoenergy Sci. Eng.* **2023**, *221*, 111264–111271. [CrossRef]
17. Dreiser, C.; Krätz, L.J.; Bart, H.J. Kinetics and Quantity of Crystallization Fouling on Polymer Surfaces: Impact of Surface Characteristics and Process Conditions. *Heat Transf. Eng.* **2015**, *36*, 715–720. [CrossRef]
18. Pääkkönen, T.M.; Riihimäki, M.; Simonson, C.J.; Muurinen, E.; Keiski, R.L. Modeling $CaCO_3$ Crystallization Fouling on a Heat Exchanger Surface–Definition of Fouling Layer Properties and Model Parameters. *Int. J. Heat Mass Transf.* **2013**, *83*, 84–98. [CrossRef]
19. Macadam, J.; Parsons, S.A. Calcium Carbonate Scale Control, Effect of Material and Inhibitors. *Water Sci. Technol.* **2004**, *49*, 153–159. [CrossRef]
20. Gong, L.; Wu, F.Y.; Pan, M.F.; Huang, J.; Zhang, H.; Luo, J.L.; Zeng, H.B. Exploring the mechanisms of calcium carbonate deposition on various substrates with implications for effective anti-scaling material selection. *Pet. Sci.* **2024**, *21*, 2870–2880. [CrossRef]
21. Charpentier, T.V.; Neville, A.; Baraka-Lokmane, S.; Hurtevent, C.; Ordonez-Varela, J.R.; Nielsen, F.M.; Bache, Ø. Evaluation of Anti-Fouling Surfaces for Prevention of Mineral Scaling in Sub-Surface Safety Valves. In Proceedings of the SPE International Oilfield Scale Conference and Exhibition, Aberdeen, Scotland, 15 May 2014.
22. Keysar, S.; Semiat, R.; Hasson, D.; Yahalom, J. Effect of Surface Roughness on the Morphology of Calcite Crystallizing on Mild Steel. *J. Colloid Interface Sci.* **1994**, *162*, 311–319. [CrossRef]
23. Vazirian, M.M.; Charpentier, T.V.; de Oliveira Penna, M.; Neville, A. Surface Inorganic Scale Formation in Oil and Gas Industry: As Adhesion and Deposition Processes. *J. Pet. Sci. Eng.* **2016**, *137*, 22–32. [CrossRef]
24. Liu, Z.; Ren, L.; Zhang, B.; Jing, J.; Zhang, X.; Li, M.; Wang, H. Eco-Friendly Waterborne Superhydrophobic/Superoleophilic Feve Composite Coating with Prolonged Mechanochemical and Anti-Scaling Properties. *Chem. Eng. J.* **2023**, *451*, 138693–138703. [CrossRef]
25. Graham, G.M.; Goodwin, N.; Albino, E.; Guan, H.; Pinto, H.L.; Bezzera, M.C. Minimizing Scale Deposition Through Surface Enhancement in Downhole Tools. In Proceedings of the SPE International Oilfield Scale Conference and Exhibition, Aberdeen, Scotland, 14 May 2014.
26. Kukulka, D.J.; Devgun, M. Fouling Surface Finish Evaluation. *Appl. Therm. Eng.* **2007**, *27*, 1165–1172. [CrossRef]
27. Bhushan, B. *Introduction to Tribology*, 2nd ed.; Wiley: New York, NY, USA, 2013; Volume 1, pp. 1–471.
28. Gadelmawla, E.S.; Koura, M.M.; Maksoud, T.M.; Elewa, I.M.; Soliman, H.H. Roughness Parameters. *J. Mater. Process. Technol.* **2002**, *123*, 133–145. [CrossRef]
29. Backes, A.R.; Bruno, O.M. Técnicas de Estimativa da Dimensão Fractal: Um Estudo Comparativo. *INFOCOMP J. Com put. Sci.* **2005**, *4*, 50–58.
30. Yang, Q.; Ding, J.; Shen, Z. Investigation of Calcium Carbonate Scaling on ELP Surface. *J. Chem. Eng. Jpn.* **2000**, *33*, 591–596. [CrossRef]
31. Al Nasser, W.N.; Al Salhi, F.H. Kinetics Determination of Calcium Carbonate Precipitation Behavior by In-Line Techniques. *Powder Technol.* **2015**, *270*, 548–560. [CrossRef]
32. Lioliou, M.G.; Paraskeva, C.A.; Koutsoukos, P.G.; Payatakes, A.C. Heterogeneous Nucleation and Growth of Calcium Carbonate on Calcite and Quartz. *J. Colloid Interface Sci.* **2007**, *308*, 421–428. [CrossRef]
33. Callister, W. *Materials Science and Engineering: An Introduction*, 7th ed.; Wiley: Hoboken, NJ, USA, 2020; pp. 1–775.
34. Zhao, J.; Wang, M.; Lababidi, H.M.; Al-Adwani, H.; Gleason, K.K. A Review of Heterogeneous Nucleation of Calcium Carbonate and Control Strategies for Scale Formation in Multi-Stage Flash (MSF) Desalination Plants. *Desalination* **2018**, *442*, 75–88. [CrossRef]
35. Mcpherson, I.J.; Peruffo, M.; Unwin, P.R. Role of Mass Transport in the Deposition, Growth, and Transformation of Calcium Carbonate on Surfaces at High Supersaturation. *Cryst. Growth Des.* **2022**, *22*, 4721–4729. [CrossRef] [PubMed]
36. Contreras, V.; Paz, P.; Netto, T.A. Experimental Analysis of Inorganic Scale Deposition in Pipes: Mesoscale Flow Loop Development and Case Study. *J. Pet. Sci. Eng.* **2022**, *209*, 109776–109781. [CrossRef]
37. Hamm, L.M.; Giuffre, A.J.; Han, N.; Tao, J.; Wang, D.; De Yoreo, J.J.; Dove, P.M. Reconciling Disparate Views of Template-Directed Nucleation Through Measurement of Calcite Nucleation Kinetics and Binding Energies. *Proc. Natl. Acad. Sci. USA* **2014**, *111*, 1304–1309. [CrossRef]

38. Cosmo, R.D.P.; Pereira, F.D.A.R.; Ribeiro, D.D.C.; Barros, W.Q.; Martins, A. Estimating CO_2 Degassing Effect on $CaCO_3$ Precipitation Under Oil Well Conditions. *J. Pet. Sci. Eng.* **2019**, *181*, 106207–106215. [CrossRef]
39. Loureiro, J.B.R.; Gonçalves, A.S.; Souza, B.G.B.; Pepe, I.M.; Demetino, G.G.; Soares, L.C.S.; Silva, C.E.T.; Soares, L.L.O.; Santos, H.F.L.; Castro, B.B.; et al. Large Scale Pipe Flow Experiments for the Evaluation of Non-Chemical Solutions for Calcium Carbonate Scaling Inhibition and Control. *SPE Int. Oilfield Scale Conf. Exhib.* **2022**, *28*, 201–2014.
40. Moriconi, L.; Nascimento, T.; de Souza, B.G.B.; Loureiro, J.B.R. Top-down model of calcium carbonate scale formation in turbulent pipe flows. *Therm. Sci. Eng. Prog.* **2022**, *28*, 101141–101151. [CrossRef]
41. Graham, G.M.; Collins, I.R.; Stalker, R.; Littlehales, I.J. *The Importance of Appropriate Laboratory Procedures for the Determination of Scale Inhibitor Performance*; International Symposium on Oilfield Scale: Aberdeen, UK, 20 January 2002.
42. Bezerra, M.C.M.; Rosario, F.F.; Rosa, K.R.S.A. Scale management in deep and ultradeep water fields. In Proceedings of the Offshore Technology Conference Brasil, Rio de Janeiro, Brazil, 29 October 2013.
43. Aljeban, N.; Al-Harbi, B.; Chen, T.; Balharth, S. Systematic calcium carbonate scale risk evaluation from downhole to topside flowline. In Proceedings of the SPE Asia Pacific Oil and Gas Conference and Exhibition, Virtual, 12 December 2020.
44. Moghadasi, J.; Jamialahmadi, M.; Müller-Steinhagen, H.; Sharif, A.; Ghalambor, A.; Izadpanah, M.R.; Motaie, E. Scale formation in Iranian oil reservoir and production equipment during water injection. In Proceedings of the SPE International Oilfield Scale Conference and Exhibition, Aberdeen, UK, 29 January 2003.
45. Cosmo, R.D.P.; Pereira, F.D.A.R.; Soares, E.J.; Martins, A.L. Modeling and validation of the CO_2 degassing effect on $CaCO_3$ precipitation using oilfield data. *Fuel* **2022**, *310*, 122067–122077. [CrossRef]
46. Al-Anezi, K.; Johnson, D.J.; Hilal, N. An atomic force microscope study of calcium carbonate adhesion to desalination process equipment: Effect of anti-scale agent. *Desalination* **2008**, *220*, 359–370. [CrossRef]
47. Martins, A.L.; Santos, H.F.; Castro, B.B.; Gonçalves, A.S.; Maffra, D.A.; Loureiro, J.B. Large Scale Laboratory Tests for Calcium Carbonate Scaling in Sliding Sleeve Valves. In Proceedings of the SPE International Oilfield Scale Conference and Exhibition, Virtual, 24 January 2020.
48. Herz, A.; Malayeri, M.R.; Müller-Steinhagen, H. Fouling of roughened stainless steel surfaces during convective heat transfer to aqueous solutions. *Energy Convers. Manag.* **2008**, *49*, 3381–3386. [CrossRef]
49. *ISO 21920-1:2021*; Geometrical Product Specifications (GPS)—Surface Texture: Profile—Part 1: Indication of Surface Texture. International Organization for Standardization: Geneva, Switzerland, 2021.
50. *ASTM C1624-22*; Standard Test Method for Adhesion Strength and Mechanical Failure Modes of Ceramic Coatings by Quantitative Single Point Scratch Testing. ASTM International: West Conshohocken, PA, USA, 2022.
51. *ASTM G171-03(2017)*; Standard Test Method for Scratch Hardness of Materials Using a Diamond Stylus. ASTM International: West Conshohocken, PA, USA, 2017.

Disclaimer/Publisher's Note: The statements, opinions and data contained in all publications are solely those of the individual author(s) and contributor(s) and not of MDPI and/or the editor(s). MDPI and/or the editor(s) disclaim responsibility for any injury to people or property resulting from any ideas, methods, instructions or products referred to in the content.